

Detecting molecular separation in nano-fluidic channels through velocity analysis of temporal image sequences by multivariate curve resolution

Kateryna Artyushkova · Anthony L. Garcia · Gabriel P. L pez

Received: 20 October 2009 / Accepted: 10 December 2009 / Published online: 30 December 2009
  Springer-Verlag 2009

Abstract In this study, we report on a method of determining individual velocities of molecular species being separated in a fluid medium within array of nanofluidic channels that can be useful in the detection of molecular species. The method is based on the application of multivariate image analysis methods, in this case principal component analysis and multivariate curve resolution, to temporal image series capturing multiple species moving through the medium. There are two novel and unique advantages of the reported method. First, it is possible to identify transport velocities of different molecular species, even those tagged with the same fluorophore. And second, the velocity determination can be made before there is any visual separation of the species in the medium at the very initial stages of separation. The capability of the methodology to detect the separation of species without fluorescent labeling and to provide an accurate ratio of their velocities even at the very early pre-visual stage of separation will significantly optimize separation experiments and assist in fast and accurate detection of analytes based on micro- and nano-fluidics assays. The presented method can be practiced in connection with various molecular separation techniques including, but not limited to, nano-channel electrophoresis, microchannel capillary electrophoresis, and gel electrophoresis.

Keywords Nanofluidics · Flow visualization · Velocimetry · Multivariate image analysis · Multivariate curve resolution (MCR)

1 Introduction

The ability to measure fluid velocity is important for realizing a full potential of micro- and nano-fluidics, especially for assays, where multiple screening events are required. Recent work has demonstrated that confinement of electrokinetic molecular transport in fluidic channels with transport-limiting pore sizes of nanoscopic dimensions (~ 100 nm) gives rise to unique molecular separation capabilities (Garcia et al. 2005; Yuan et al. 2007). A distinct characteristic of nanofluidic channels is that the transport-limiting channel dimension is comparable to the thickness of the electrical double layer near the interface of electrolyte solution and channel surface. Due to their comparable length scales, the electrical double layers of opposing channel walls can be close to each other or can slightly overlap. This proximity of electrical double layers results in a velocity profile following the shape of the electrostatic potential distribution along the cross-sectional plane of nanochannels (Oh et al. 2009; Petsev 2005). In the negatively charged channels, nanoconfinement and interactions between the respective solutes and the channel walls give rise to higher electroosmotic velocities for the negatively charged dye than for the neutral dye, toward the negative electrode, resulting in an anomalous separation that occurs over a relatively short distance (<1 mm) (Garcia et al. 2005). Understanding fluid and molecular transport in nanoscopic channels is a tremendous challenge because of the lack of experimental methods that are available for interrogating the positions and trajectories of

K. Artyushkova (✉) · G. P. L pez
Chemical and Nuclear Engineering Department, The University of New Mexico, 209 Farris Engineering Center, Albuquerque, NM 87131, USA
e-mail: kartyush@unm.edu

A. L. Garcia
Sandia National Laboratories, Albuquerque, NM 87185, USA

molecules at sub-wavelength dimensions. Silicon-based T-chips containing an array of parallel nanochannels can be used to study the electrokinetic transport of fluorescent dyes in nanochannels. Fluorescent imaging using confocal microscopy is an excellent method for the direct observation of molecules in chemical separation due to its high sensitivity (Lowry et al. 2002). While the details for the flow profiles in the individual nanochannels are below the resolution limit of optical microscopy, average velocities of dye fronts within array of nanochannels can be monitored and provide insight into the electrokinetic transport mechanisms in the nanochannels. Simultaneous transport of positive and negative dyes in the channels provides better understanding of the electrokinetic mechanism of separation.

Microscale flow visualization methods applied for the determination of fluid velocity in microsystems is well addressed (Bellan et al. 2007; Grega et al. 2007; Sinton 2004; Natrajan and Christensen 2007; Markov et al. 2004; Bergsma et al. 2001). The task of change detection is to determine how much and in what direction has a pixel changed. Velocity estimation methods can be roughly divided into two groups: particle and model-based spot tracking methods (Bellan et al. 2007; Grega et al. 2007; Natrajan and Christensen 2007; Markov et al. 2004; Ditrach and Schwille 2002) and image derivative-based methods like optical flow (Horn and Schunck 1993; Tagliasacchi 2007). The types of movement generally studied by these methods usually involve discrete object or multiple objects that are changing their location within an image field of view. The particles are often added into the fluid, such that the transport is detected but not altered. Spot-tracking methods rely on accuracy of the segmentation of characteristic objects, such as particles or cells. No segmentation is needed for optical flow methods. The overall or “average” velocity describing all objects moving within a system of study is obtained by these methodologies. The movement of dye front within an array of nanochannels is quite different—there are no discrete objects for which intensity profiles can be monitored as a function of time. Front moves as a plug profile in the array of nanochannels. With time, the nanochannels are being filled up with the dye. Moreover, “average” or “overall” velocity is not a useful parameter in studying separation of species moving with different velocities within micro- and nanochannels. For such type of movement, velocity calculation is usually done manually through plotting a large number of horizontal profiles within individual red (R) or green (G) components of each image capturing only one type of fluorescing species (red or green) and determining the position of the dye front from those horizontal profiles. This is time-consuming and somewhat subjective procedure. Large number of horizontal profiles needs to be

processed to obtain an accurate representation of average velocity of the front of each dye.

Among multivariate analysis methods that may be tested for velocity estimation are principal component analysis (PCA) and multivariate curve resolution (MCR) (Jaumot et al. 2004; Adams 1995; Malinowski 1991). These methods allow to fully exploiting the data by analyzing all pixels within images and using the temporal dimension, in contrast with manual methods, where a limited number of horizontal profiles are processed. Previous studies have found that PCA is useful to extract change information from multitemporal remote-sensing data (Gurden et al. 2003). The higher order components retain information on changes. For example, in IR image sequences higher PCs showed a dynamic scene behavior during time variant heating by solar illumination (Sahouria and Zakhor 1999). All two-way multivariate analysis methods such as PCA and MCR suffer from rotational ambiguities (Malinowski 1991; Tauler et al. 1995). MCR allows partially overcoming this problem by introducing physically meaningful constraints such as nonnegativity. This also assists in the problem of identification and interpretation of loadings and scores with negative values extracted by PCA (Tauler et al. 1995; Windig and Guilment 1991; de Juan et al. 2004).

In this report, we demonstrate that identification of transport velocities of different molecular species can be accomplished by the use of multivariate image analysis techniques. Through application of PCA and MCR to a set of confocal temporal image sequences, obtained for different sizes of nanochannels at different experimental conditions, the criteria for velocity estimation was developed and validated. Influence of image sequences properties and preprocessing on the criteria was estimated as well.

2 Experimental

2.1 Data acquisition

Silicon-based T-chips, integrating an array of parallel nanochannels with microchannels, for fluid control, and macroscopic injection ports, used in this study are shown in Fig. 1a. A cross-sectional scanning electron micrograph of a small number of nanochannels in one of the T-chips used for this study is shown in Fig. 1b. In this chip, the channels are approximately 50 nm wide by 500 nm deep, and are on a 400-nm pitch.

Electrokinetic separations used a buffer containing 0.25 M *tris*-(hydroxy)aminomethane hydrochloride and 1.92 mM glycine at pH 8.8 (*viz.*, a 1/100 dilution of the standard poly(acrylamide) gel electrophoresis buffer). Solutions of dyes (rhodamine B (MW = 479 Da) and Alexa 488 maleimide (MW = 720 Da), Molecular Probes

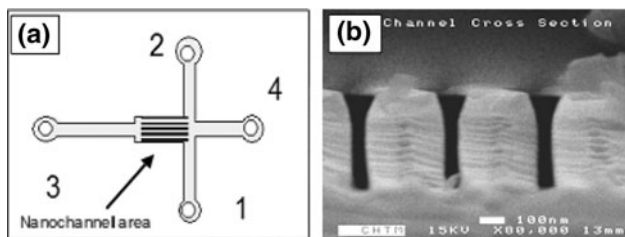


Fig. 1 **a** Top view (schematic) of the integrated chips. The holes are numbered for reference, and nanochannel area is noted. The channels are 3 cm long from well 3 to well 4, and 2 cm from well 1 to well 2. **b** SEM image of the cross section of the nanochannel array (50 nm wide nanochannels) in a chip taken after experiments were performed showing a Pyrex lid bonded to the oxidized silicon trenches to form channels

Inc., Eugene, OR, USA) were prepared in this buffer, each at a concentration of 5 mg/ml. At pH 8.8, rhodamine B is neutral and Alexa 488 maleimide has a charge of -2 . They will be referred to as Red and Green throughout the article.

Electrode 2 (see Fig. 1a) was grounded, whereas the remaining 3 electrodes were attached to the outputs of three separate DC power supplies. The chip was filled with buffer (no dyes) via capillary action from well 3 and placed under an upright, laser-scanning confocal microscope (Zeiss Axioskop with an LSM5 scanning head). Two excitation lasers of 488 and 543 nm wavelength were used. Two separate detectors are used to detect fluorescence from Alexa 88 dye by bandpass filter (505–530 nm) captured as Red channel and from Rhodamine dye by a long pass filter (>560 nm) captured as Green channel.

10 μ l of a 1:1 mixture of the two dye solutions was introduced into well 1, and initially Electrode 1 was set to +30 V relative to Electrode 2 (electrodes 3 and 4 were set to 0 V), so that the solution moved from well 1 toward well 2 by electroosmosis in the microchannel. Separation of the two dyes was not observed in the microchannels during this step. Once the dye mixture (as monitored by fluorescence microscopy) reached the T-intersection, Electrode 1 was set to 0 V and Electrode 4 was set to a varied value of voltage, V , so the fluid flowed toward well 3 through the nanochannels via electroosmosis. The evolution of the dye fronts through the nanochannel array was followed by acquiring a series of confocal images 2 mm down the microchannel length.

Three sizes of nanochannels were studied: 50, 90, and 160 nm. For 50 nm, three voltages of 15, 20, and 60 V were used. For 90 nm chip, 40 V was used, whereas for 160 nm, three voltages of 8, 24, and 50 V were used. In all of these experiments, the neutral Rhodamine (Red) and negative Alexa 88 (Green) dyes were injected simultaneously. Time difference between consecutive image acquisitions for 160 nm channels is 7.87 and 5 s for 50 and

90 nm channels. 512×512 pixel confocal images representing 2×2 mm² were acquired.

Due to quite low concentration of dyes used, effect of concentrated regions of dye on local ionic strength of the buffer and thus electric field is negligible.

2.2 Manual image processing

Acquired confocal images cover an area of 2×2 mm², whereas microchannel with an array of nanochannels is narrower than that in vertical dimension, being approximately ~ 0.85 mm. This results in black background above and below the microchannel, which was removed by cropping all the images to the area containing only microchannel with array of nanochannels. For consistency, it was insured that all resulted cropped image sequences had the same dimensions. For manual calculations of velocity, images were smoothed using Gaussian smoothing, in order to provide a clear front of the profile for accurate distance calculations. For subset of images (~ 5 – 10 depending on overall number of images in the experiment), overall intensity profiles were calculated. Specifically, for image with dimensions of $[n \times m]$, sum of n vectors of $[1 \times m]$ dimensions resulted in a vector, representing an overall intensity profile. Most intensity profiles produced a “step-like” spike in intensity which made it easy to determine the position of the front (Fig. 2). Horizontal lines were drawn to determine the position of the dye front as shown in Fig. 2. The positions of the dye fronts were noted in at least five places (i.e., five horizontal line profiles taken) for each image and the number of pixels the front has moved from image N to image M was calculated. Finally, the dye velocity was determined by dividing distance the front has

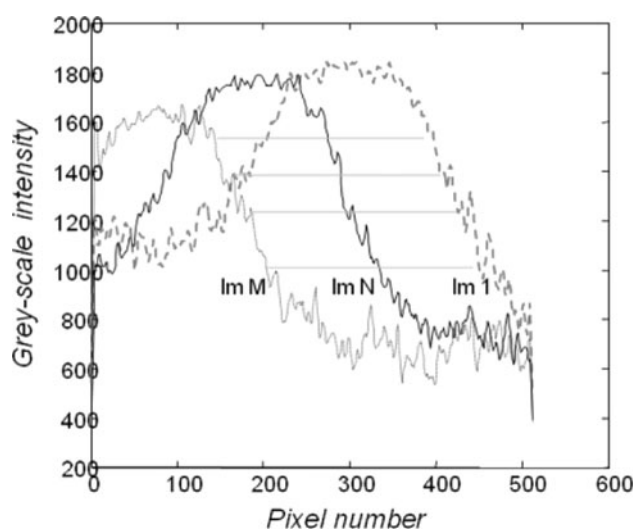


Fig. 2 Manual determination of velocities. Overall intensity profiles are plotted for each image. Multiple horizontal lines are drawn to calculate number of pixels shifted from images 1 to N

Table 1 Properties of confocal image temporal sequences

Nanochannel size (nm)	V	Component	Total # of images	Total t (s)	Distance (μm)
50	15	G	36	180	2000
		R			616
	20	G	25	125	2000
		R			312
60	G	36	180	2000	
	R			616	
90	40	G	30	150	625
		R			586
160	8	G	100	787	2000
		R			2000
	24	G	59	464	2000
		R			2000
	50	G	40	315	2000
		R			2000

moved by the time difference between the images. The reported manual dye velocity is an average of the velocities calculated in this manner for all five line profiles and all time intervals.

The distance traveled by the dye was manually evaluated from the images as well. For most of the image sequences, the first image has a front of the dye just entering the array, and the front exits the array prior to the last image in the sequence. It is accomplished by supervising acquisition and turning confocal image acquisition on and off. For such data sets, dye front travels through the full channel length, i.e., 2000 μm . For some image sequences, the first image may have the front within nanochannels by some distance or the front may not reach the exit of the array by the end of acquisition. In these image sequences, the distance traveled was evaluated from horizontal profiles as described above.

Table 1 shows image sequences acquired with total number of images in them, total time of acquisition, and distance traveled by the dye determined from horizontal profiles.

2.3 Data analysis approach

PCA, the most widely used MVA method, is often the starting point in multivariate data analysis (Malinowski 1991). PCA transforms the experimental data matrix into a smaller number of principal components, each having a score and loading associated with it. Each loading has an eigenvalue that describes, in principle, the amount of variance explained by the loading. The primary components corresponding to the largest r eigenvalues represent the set of components that span the true subspace for the data,

whereas the remaining components, each describing a low variance, represent the noise in the data set. A variety of different methods have been developed as an extension of PCA in order to extract positive, and potentially more chemically meaningful, components (Tauler et al. 1995). One of the methods, MCR, refers to a group of techniques which recover the spectral and time or intensity profiles of components in an unresolved and unknown mixture for which no prior information is available about the nature and composition of these mixtures. MCR utilizing an alternating least squares (ALS) algorithm can use information from PCA for initialization and local physical constraints. Both methods are quite different in the way they treat data, i.e., PCA explains variability in the data, whereas MCR separates data by their purity; PCA orders principal components in the order of decreasing variance, where the first captures the most variability in the data, the second captures the next most variance, etc., whereas MCR finds r most pure variables with no specific order of significance. For developing a stable criterion for velocity calculations based on MVA method, it is important to have consistent order of the extracted components. One could have created MCR models using r randomly generated vectors for initialization, but then the order of components may have been different from one image sequence to another, making it impossible to find the same criteria indicative of velocity or ratio of velocities. PCA is therefore used as a first step, where principal components, ordered by the variance they capture, are used for MCR initialization.

For both PCA and MCR, each image $[n \times m]$ is first unfolded into a vector $[n^*m \times 1]$, and an algorithm using r components is applied to a matrix formed by combining the vectors for p variables (times) into a 2D matrix $[n^*m \times p]$. The resulting score vectors $[n^*m \times r]$ are then converted back to an image format $[n \times m \times r]$. Because of this transformation, PCA and MCR do not take into account spatial interrelationship between pixels in images, which may benefit the average velocity calculations, as discussed below.

As will be seen from images in sequences in Sect. 3, dye enters individual nanochannels at slightly different times, so the front is not uniformly distributed along the vertical dimension of the array. Diagram shown in Fig. 3 shows the reason for curved shape of the front. The east and west microchannels are initially filled with dye, while the north microchannel is not. When the chip is left for some time, the excess dye diffuses from the center, leaving some dye in the arms. When the dye is being introduced into nanochannel, it enters sides first, end then the center, resulting in an uneven profile as is observed in all images herein. A care, thus, should be taken when velocity is calculated manually to obtain an accurate representative of average velocity of the dye front, which is accomplished by

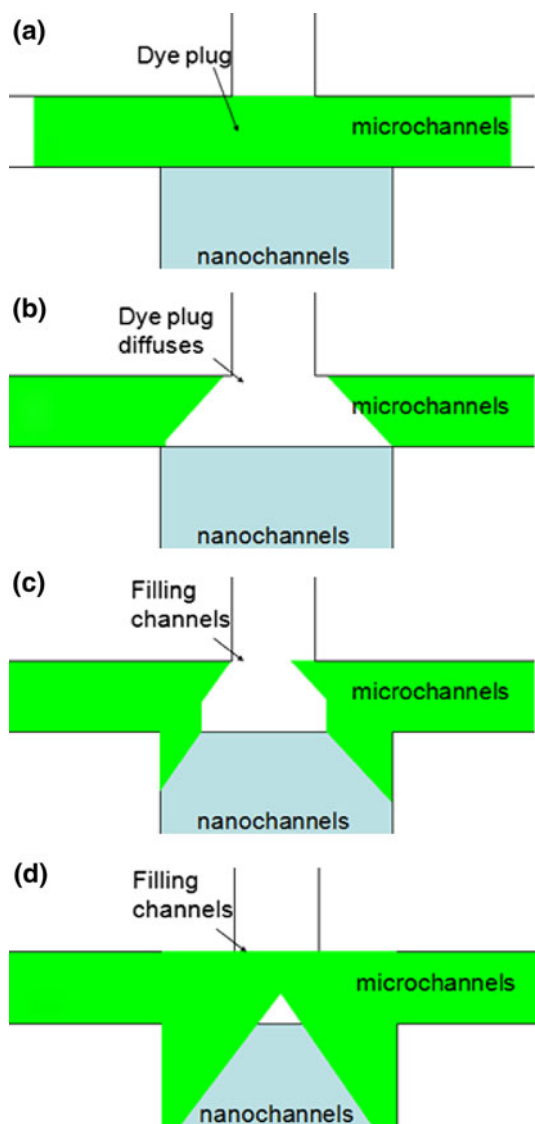


Fig. 3 Diagram of filling the nanochannels with dye resulting in uneven front

averaging results from five profiles. In case of PCA and MCR, though, the spatial relationships are ignored, while the overall image intensity is used to model a difference between images at each two consecutive times, therefore serving as accurate representation of “overall” or “average” intensity changes with time.

RGB tiff images were opened in Matlab (MATLAB). Green and red components were saved in separate image sequences. RGB tiff images containing both red and green components (both dyes) were converted to gray-scale and saved as separate image sequence (referred to as Mix). For multivariate analysis, original images with no smoothing were used to eliminate introduction of any changes in intensity within images.

Image PCA from PLS Toolbox 4.3. (Eigenvector Research) and MCR-ALS (MCR-ALS, <http://www.ub.edu/mcr/download.htm>) were used.

The number of principal components determined for most image sequences from scree plot was determined to be 3. PCA, thus, was applied using three PCs for all image sequences for consistency. No scaling of data was chosen in PCA in order to extract loadings most resembling temporal profiles in which absolute image intensity is compared to a background intensity of 0, rather than to a mean intensity of 0, which would be the case if the data would be mean centered or autoscaled.

The extracted temporal profiles were then used as an initialization for MCR-ALS algorithm. Nonnegativity constraints in both spatial and temporal directions were applied in MCR. We will refer to the output from MCR to as “pure images” and “pure profiles,” according to terminology of MCR as method based on *purity* (Tauler et al. 1995). Velocity calculations from MCR results are discussed in Sect. 3.

3 Results and discussion

3.1 Original image sequences

Figure 4 shows a subset of 5 images out of 100 images for Green component image sequence acquired from 160 nm chip at 8 V. The dye front is moving from right to left side of the image within the array of nanochannels. Increase in intensity with each consecutive image is observed. At image 75 (1d), the array is completely filled with the dye. By the end of the run (image 100), the intensity has decreased at the entrance side (right). In Red component image for the same experiment (Fig. 5), the dye front

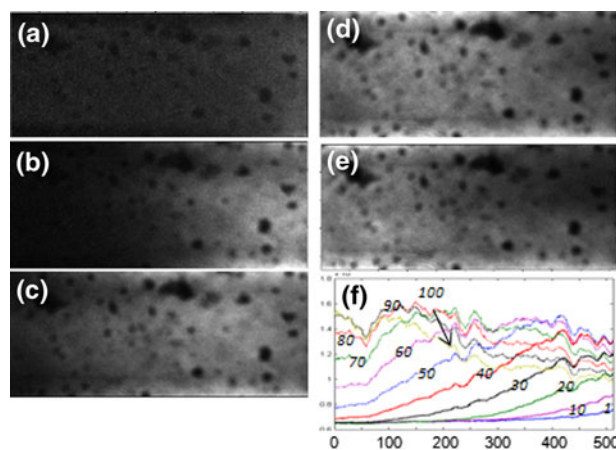


Fig. 4 Original confocal images from Green component, 160 nm 8 V. **a** # 1, **b** # 25, **c** # 50, **d** # 75, and **e** # 100 sequences are displayed. **f** Averaged horizontal profiles for images # 1, 10, 20, 30, 40, 50, 60, 70, 80, 90, and 100

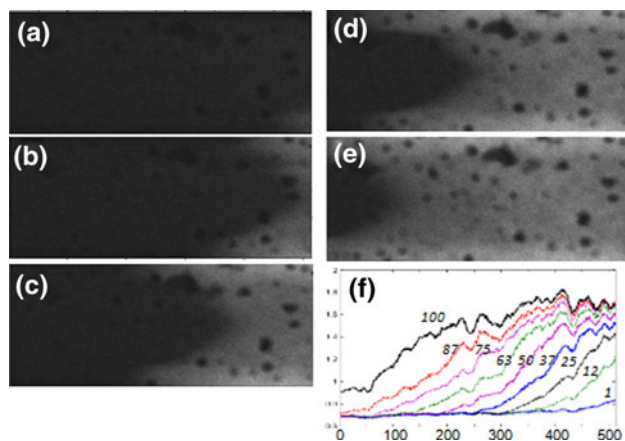


Fig. 5 Original confocal images for Red component, 160 nm 8 V. **a** # 1, **b** # 25, **c** # 50, **d** # 75, and **e** # 100 sequences are displayed. **f** Averaged horizontal profiles for images 1, 12, 25, 37, 50, 63, 75, 87, and 100

propagates by some distance into a channel, while intensity of the dye at the entrance side of the image does not decrease. These two types of temporal behavior, that were observed throughout all image sequences analyzed, are better visualized by plotting average horizontal profiles for series of images. In Fig. 4f, the profile for the first image (Green component) is a flat line. For image 10, an increase in intensity at the entrance (right) side of the image is visible. This increase continues with time, until the dye front has reached the exit (left side) and moved away from the right side which is visible in decrease of intensity at the entrance side for the last image. For the second type of data set (Red component in Fig. 5f), the dye front moved into the nanochannels by some distance and did not leave the entrance side.

Dependence of image analysis methodology developed herein on these two types of behavior of dye front must be considered, as will be discussed later. Another parameter that may change the output from PCA/MCR is visibility of the dye front within the first image in the sequence. The first image in sequence for Green channel from 90 nm chip at 40 V (Fig. 5a) has a dye front within a channel. In

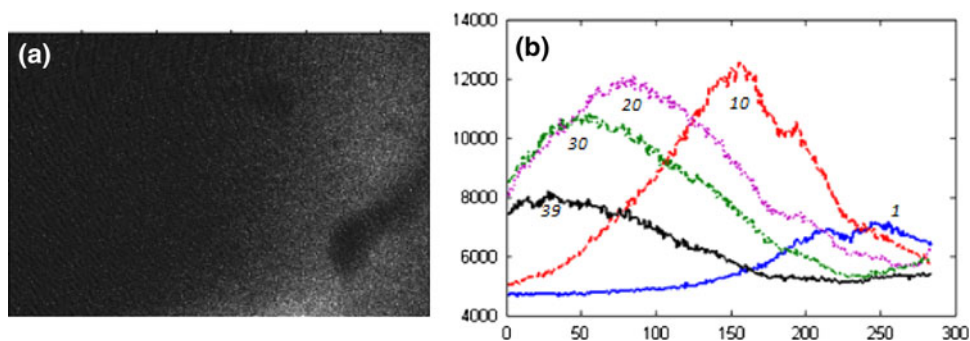
horizontal average profile for this image (Fig. 6b), it is seen that at the very beginning of image acquisition, the dye front has already moved in the nanochannels by approximately 100 pixels.

Dark spots are observed in all images due to salt deposits on the surface of the glass coverslip, which are a byproduct of the anodic bonding process of permanently bonding the silicon wafer and Pyrex glass together during microchip build-up. These spots are at exactly the same positions for all images in the sequence, thus, they have exactly the same contribution to the total intensity of all pixels for each image in the sequence. These spots do show up in the horizontal profiles, complicating accurate manual calculations of velocities even more. PCA, as a method using integrated total intensity as an input for calculations, is not affected by presence of these spots, as the same percentage of the signal (dark pixels in the images due to the spots) contributes into total image intensity for each image in the sequence and, thus, is taken into account.

In Red component image sequence (Fig. 5), another important feature must be noted. The dye front advances more into nanochannels at the top and bottom of the array in comparison with the middle part of the image. The reason for that is discussed in Sect. 2 and shown in diagram in Fig. 3. As was discussed in Sect. 2, when performing manual calculations of velocity for such data set, all parts of the image must be included to obtain a real average representative of front movement. MVA methods, however, due to the fact that they do not model spatial relationship, take care of this problem automatically, as full image is used for modeling purposes.

Images in Fig. 7 show a subset of RGB and gray-scale images of original TIFF images capturing movement of both dyes. In RGB images, one can distinguish the faster movement of the green dye relatively to the red. In gray-scale images, however, no distinction is possible, as intensities of both channels are just summed up. It is intriguing to test whether MVA methods would be able to detect movement of both dyes within gray-scale images due to perturbation in flow of one dye by the other dye moving with different velocity.

Fig. 6 Original confocal image for Green component, 90 nm 40 V. **a** First image and **b** averaged horizontal profiles for images # 1, 10, 20, 30, and 39



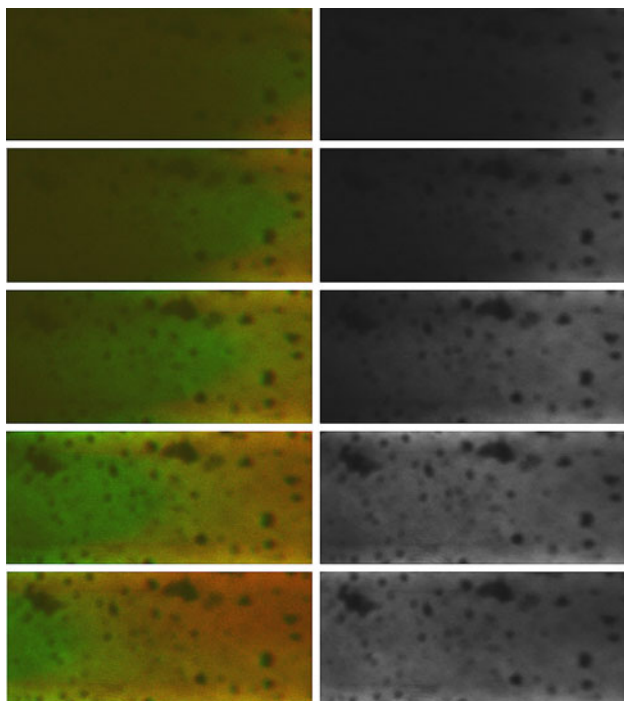
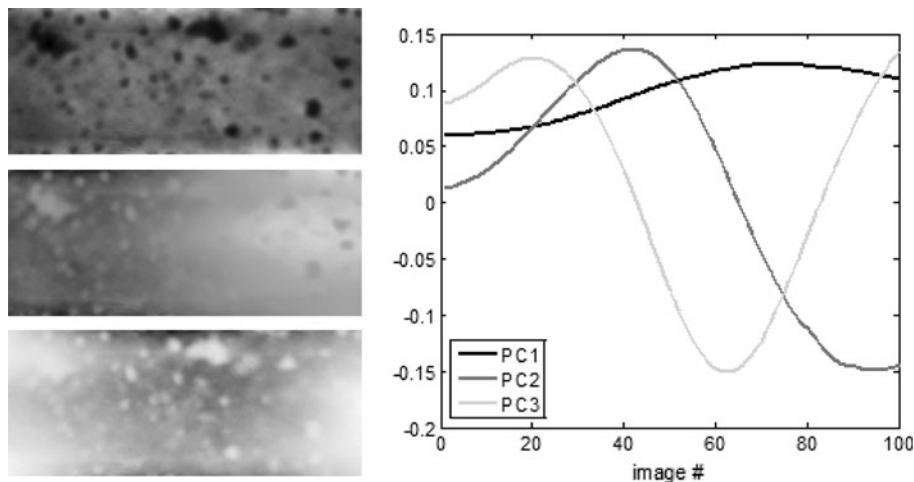


Fig. 7 Original confocal images capturing both dyes for 160 nm 8 V. *Left column* RGB images. *Right images* gray-scale images. From top to bottom: images # 1, 25, 50, 75, and 100 are shown

3.2 Application of MVA methods to image sequences

Figure 8 shows results of PCA applied to temporal sequence of 100 Green component images for 160 nm channel at 8 V using no scaling option. Three PCS are extracted. The first PC loading increases gradually and reaches a maximum at around image 72. Its score image looks like completely filled channel. The second PC loading increases and reaches maximum at image 42 and then decreases down to minimum at image 95. Its score image looks like an inverse of the last image in the

Fig. 8 PCA results for image series from Green component, 160 nm 8 V. Three scores images and loading are shown



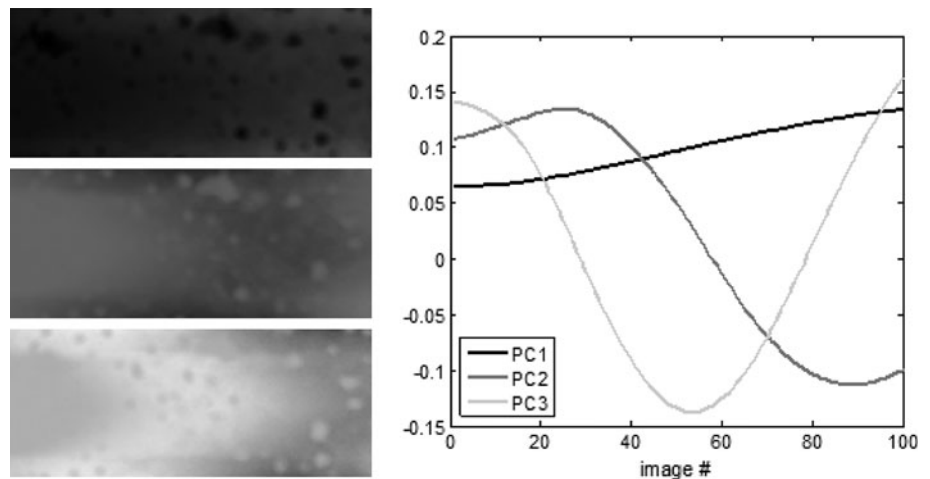
sequence. The third PC loading has a minimum at around image 61 and reaches the same level at the beginning and the end of the run. The score image for this component looks like an inverse of the first PC. Negative values within images and loadings make it hard to interpret and identify extracted PCs. Results of PCA applied to the Red component from the same data sets (Fig. 9) are similar to that of the Green component, except the second PC loading does not have such pronounced maximum. The first PC also increases with time but does not have maximum as in case of Green component. It is due to the fact that dye is not leaving the nanochannels as it does in the case of green dye. The first PC score looks like the last image in the sequence. Interpretation of the second and third components is also complicated due to inverted images.

Inverted images and negative values of intensity in loadings extracted by PCA make it difficult to interpret the results and therefore have a complete grasp of the developed algorithm and understanding of the capabilities of MVA to extract ratios of velocities from temporal image sequences. Application of physically meaningful constraints, such as nonnegativity of intensity values in both images and profiles, which is possible in MCR-ALS, solves this problem and at the same time tries to overcome the problem of rotational freedom from which all two-way MVA methods suffer.

As was discussed in Sect. 2, principal component loadings were used as initialization of MCR algorithm. This is a beneficial alternative to using randomly generated vectors, as this insures the same order (in the order of decreasing variance as determined by PCA) of extracted pure components for all image sequences which is critical for developing a consistent and stable criteria for velocity determination.

MCR results for Green, Red, and Mix component from the same data set are shown in Fig. 10. The first pure image represents filled nanochannels, second pure component

Fig. 9 PCA results for image series from Red component, 160 nm 8 V. Three scores images and loading are shown



represents half-way filled, and the third one represents the last image in the data set, when dye has moved out from the channel. For Red component images (Fig. 10b), there is an interesting observation in the third PC. It looks like the last image in the sequence with dye front moved out from the entrance part of the channel, which is not observed in original image. Both green and red dyes were analyzed simultaneously, so movement of the green dye is reflected in the third component extracted from Red channel due to disturbance of the flow and thus intensity of the image.

For all image sequences analyzed (seven data sets with Green, Red, and Mix channels) for all three nanochannel sizes and all voltages, similar trends in MCR pure temporal profiles are extracted. The first PC has a maximum, the second has a maximum and a minimum, and the third has a minimum at some image number. In addition, there are four intersections, one for the first with the second, one for the third with the second and two for the first and the third pure components. For example, MCR model obtained from Green image sequence for 160 nm, 8 V setup provides three pure profiles as a function of image number, as shown in Fig. 10a. The first PC has a maximum at image 70, the second has a maximum around image 40 and a minimum around image 87, and the third PC has a minimum at image 51. PC1 intersects PC2 at image 54, PC1 intersects PC3 at images 33 and 80, and PC2 intersects PC3 at image 67. These minimums, maximums, and intersections of profiles provide equivalent of the time (image number multiplied by time lap between images during acquisition) that may be related to the velocity (time divided by the distance the dye front has traveled).

Table 2 shows image numbers for minimum, maximums, and intersections of components extracted from MCR applied to image sequences as shown in example above. Note that Table 2 shows only a subset of results from three data sets out of seven analyzed as described in Sect. 2. Image number values listed in Table 2 extracted

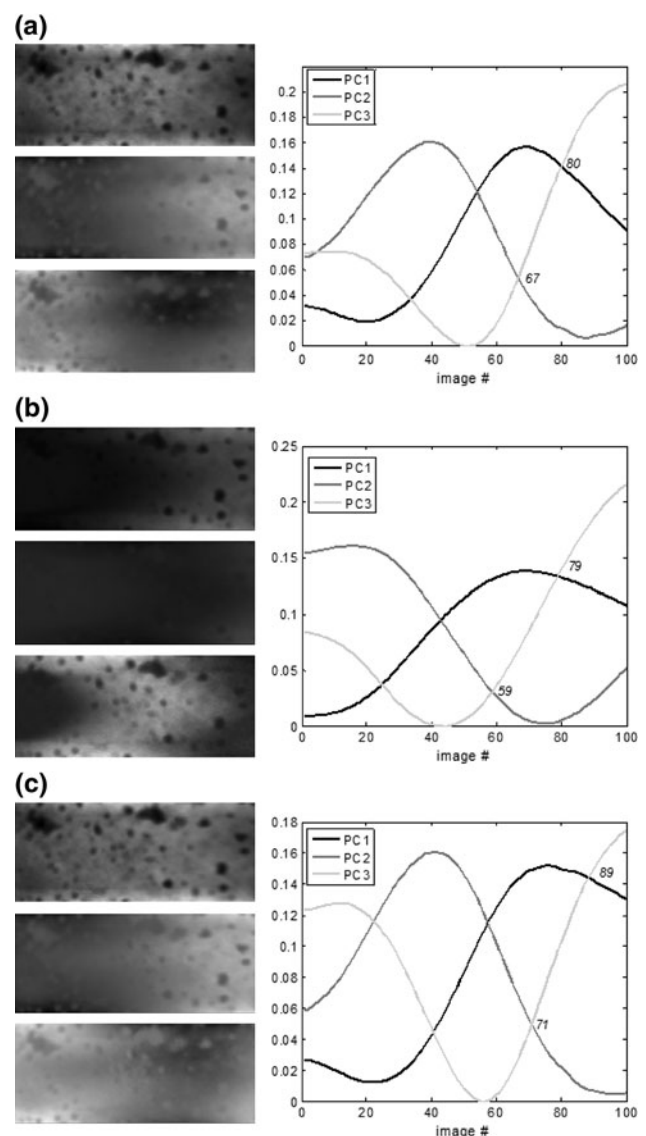


Fig. 10 MCR results for image series **a** Green, **b** Red, and **c** Mix (RGB converted to grayscale) at 160 nm 8 V. Three pure images and pure profiles are shown

from MCR temporal profiles (minimums/maximums and intersections of pure components) were multiplied by the time difference between each image in the sequence in order to obtain the total time, t (seconds), of movement. Velocities, v , were then calculated by dividing distances traveled by the dye as determined from images manually (Table 1) by time, t . These velocities were then compared with the velocity determined manually from horizontal line profiles. From this comparison, it was determined that intersections of the PC3 with the PC1 and the PC2 temporal pure profiles extracted by MCR provide an estimate of velocity of both dyes within each single (R and G) and mixed component image. The third component represents the last image in image sequence indicating the end of the experiment, when all movement of the dyes has stopped. There are two points of intersect for PC1 and PC3 temporal profiles extracted by MCR. The first appears when the PC1 component just starts increasing and the PC3 component starts decreasing. The second point of intersect is located where the first component starts decreasing after reaching a maximum, whereas the third component increases after reaching a minimum. This point representing an image at which the slower-moving dye has moved through the channel, reflecting velocity of a slow-moving dye. There are two intersection points between second and third components as well. The first appears at the very beginning of the separation, whereas the second represents the time at which the faster-moving dye passed through the channel, reflecting velocity of fast-moving dye.

As seen from Table 2, the image numbers for intersections determined from each single channel and mixed channel are a little bit different. The slower the velocity (the larger the number of images in acquired sequence needed to capture the complete movement of the dye through the channel), the larger the difference in absolute image numbers. The differences in velocities determined from two single component image sequences and mixed gray-scale sequence are approximately the same for all sizes of nanochannels and voltages. If one compares velocities calculated from MCR to manually calculated

ones, the error in the velocities determined from Green component (both green and red dyes), from Mix image (both green and red dyes), and from Red component (red dye) is 5–10%.

Absolute values of velocity determined through this methodology have an error due to errors in calculating an exact distance traveled and in cropping the image when the first image has a front visible in it. But the same error will contribute to a velocity determined through manual procedure. What is important, however, is that the relative times determined from MCR for slow- and fast-moving dyes will be exactly proportional to the ratio of velocities.

The steps that have to be applied in order to obtain absolute velocities and ratios of velocities from MCR model created from temporal image sequences (along with sample calculations for MCR results shown in Fig. 10a) are shown below.

1. Create PCA model using three components with no scaling.
2. Use PCA loadings as initialization into MCR–ALS.
3. Create MCR model using nonnegativity constraints.
4. Plot MCR pure temporal profiles and record image number for intersection of PC3 with PC1 and PC2 (image numbers 67 and 80, respectively).
5. Calculate ratio of velocities of slower moving dye to that of faster moving dye by dividing image number of intersection of PC3 with PC1 to that of PC3 with PC2 ($80/67 = 1.19$). Table 3 shows the ratios of velocities calculated in this way.
6. Multiply image numbers for intersections by time difference between images (7.87 s) to obtain the time of fast- and slow-moving dyes (526.6 and 629.6 s, respectively).
7. Divide the distance each dye traveled by the time calculated in step 6 ($2000 \mu\text{m}/526.6 \text{ s} = 3.8 \mu\text{m/s}$ and $2000 \mu\text{m}/629.6 \text{ s} = 3.2 \mu\text{m/s}$). Velocity calculated in this way from MCR, V_{MCR} , is shown in Table 3 in comparison with manually calculated velocity.

Table 2 Results of MCR. image numbers correspond to minimums, maximums, and intersections of extracted temporal profiles

	160 nm 8 V			160 nm 50 V			90 nm 40 V		
	Green	Red	Mix	Green	Red	Mix	Green	Red	Mix
1 max/min	70	68	23/76	22	14/32	24	11	13	10
2 max	40	16	41	13	18	13	6	7	6
2 min	87	74		29			21	24	22
3 max			56	36	12		26	4	3/26
3 min	51	44		18	26	16	8	10	9
1/2 cross	54	43	58	18	25	18	9	11	10
1/3 cross	33/80	24/79	41/89	11/29	13/31	11/30	6/19	7/22	6/21
2/3 cross	67	59	23/71	24	24	25	11	14	13

Table 3 Comparison of ratios of image numbers extracted from MCR with velocity ($\mu\text{m/s}$) ratio calculated manually

	160 nm 8 V			160 nm 50 V			90 nm 40 V		
	Image #	V_{MCR} ($\mu\text{m/s}$)	V_{man} ($\mu\text{m/s}$)	Image #	V_{MCR} ($\mu\text{m/s}$)	V_{man} ($\mu\text{m/s}$)	Image #	V_{MCR} ($\mu\text{m/s}$)	V_{man} ($\mu\text{m/s}$)
Green main	67	3.8	4	24	10.6	11	11	7.9	7
Red in green	80	3.2	3	29	8.8	9	19	4.6	4
Ratio	1.19		1.33	1.21		1.22	1.73		1.75
Green in red	59	4.3	4	24	10.6	11	14	6.2	7
Red main	79	3.2	3	31	8.2	9	22	4.0	4
Ratio	1.34		1.33	1.29		1.22	1.57		1.75
Mix green	71	3.6	4	25	10.2	11	14	6.7	7
Mix red	89	2.9	3	30	8.5	9	21	4.1	4
Ratio	1.25		1.33	1.20		1.22	1.57		1.75

Table 3 represents the ratios of image numbers obtained from 1/3 and 2/3 intersections and velocities calculated by manually for three out of seven data sets analyzed. All ratios are pretty close to those calculated by manually with an error of $\sim 5\%$. There was no dependence of difference of ratios obtained from Green, Red, and Mixed channels on nanochannel size. The ratios of images determined by MCR are more accurate than those by manually, due to what have been discussed previously, i.e., the fact that MCR uses full images to model the difference between them, whereas manual velocity is obtained by following evolution of a front at only a few places along the image and is subjective. Image sequences used herein were of high quality, so that accurate evaluation of front propagation from horizontal profiles as shown in Fig. 2 was possible, making the difference between manual and MCR velocities only $\sim 5\%$. In case of images of poorer quality, this difference is larger, to the point where it is simply impossible to calculate velocities manually as shown below in Fig. 12. MCR methodology, on the other hand, is able to extract velocity ratios even from image sequences of poor quality, as shown in Figs. 11 and 12.

Figure 11 shows MCR results from blurred image sequence in Fig. 4. By comparing these results to MCR

results from the original data set without smoothing (Fig. 10a), it can be seen that absolute values of intersections of pure components PC3 with PC2 and PC1 are shifted to a larger values, i.e., from 80 to 87 and from 67 to 71, respectively. The ratio of image numbers and thus ratio of velocities are 1.23, which is very close to that from original images, 1.19.

Figure 12 shows an example of image sequence of poorer quality from which it is virtually impossible to calculate the velocity manually. Horizontal profiles (Fig. 12a) are very noisy even for smoothed images, so it is very hard to estimate front propagation from them. MCR, however, is able to calculate the ratios of velocities of 1.3 quite successfully (Fig. 12c).

It is important to determine whether it is necessary to preprocess images prior to MCR by cropping them, so that the first image does not have the front dye visible as in Fig. 7a and the last image has the front moved all the way through the array. Image number 1 in a Green component sequence from 90 nm, 40 V has a dye front moved in by ~ 100 pixels into the channel. MCR results of original and cropped images provide trends similar to all other data sets analyzed. When the original images are used, the velocity is overestimated by almost 30%, while when the images

Fig. 11 MCR results for blurred image series Green at 160 nm 8 V. The pure images and pure profiles are shown

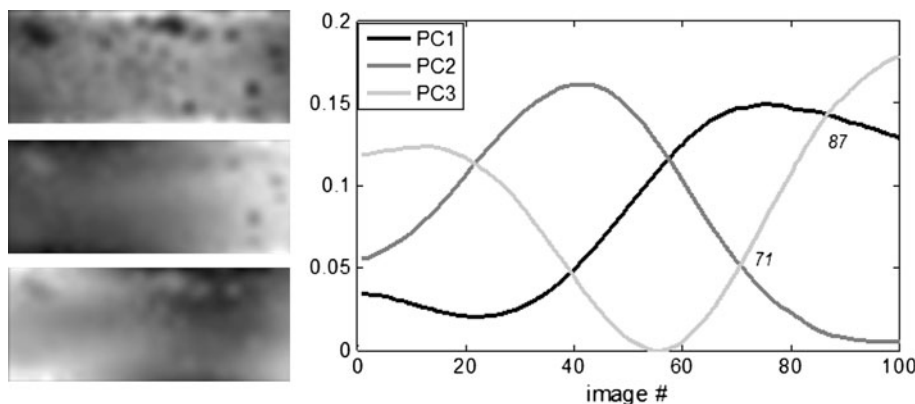
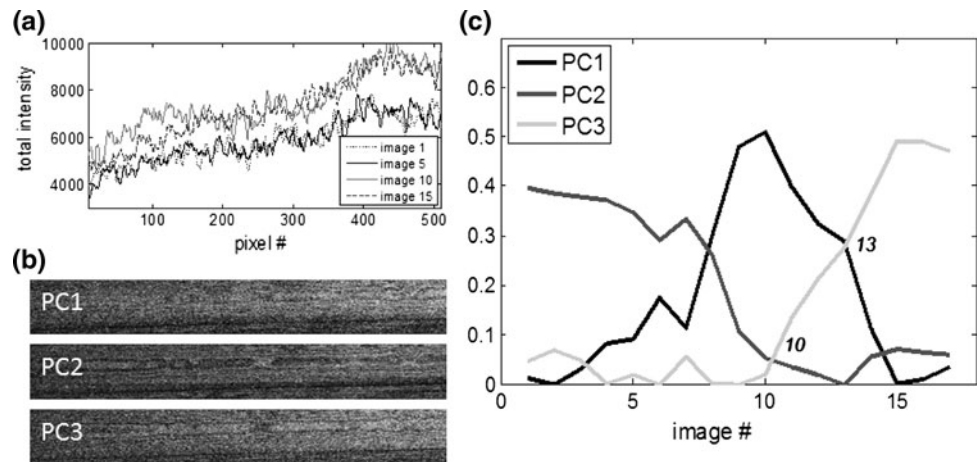


Fig. 12 Image sequence of poor quality. Red, channel, 50 nm 15 V. Horizontal profiles (a), three pure images (b), and three pure profiles (c) are shown



are cropped as discussed above, the 1/3 intersection gives an accurate estimate of velocity, taken that distance is calculated correctly. All image sequences containing a dye front in the first image in the sequence were, thus, cropped to eliminate this effect.

It was also determined that MCR results do not depend on the fact whether the dye front has reached the exit side of the image. It is very important observation, because in most of the cases when two dyes are analyzed simultaneously, by the time that one dye has reached the end, the other one has not. It is clear that is not necessary to preprocess images to be sure that both dyes have reached the exit. However, it is still critically important to accurately calculate the distance moved by the front dye in both Green and Red components.

One significant benefit of the proposed approach is that because single component image sequences (R or G) are influenced by the dye moving in the other component (G or R), application of MCR to a single channel provides information on movement of both dyes. When an RGB image representing both dyes in the array of nanochannels is converted to a gray-scale image and is analyzed by MVA methods, velocities of both dyes are extracted successfully. This potentially will allow identification of the transport velocity of different molecular species, even those tagged with the same fluorophore from RGB image sequences.

3.3 Validation for early stage of separation

All of the results discussed above are obtained from series of images where the separation between two dyes is quite clear at the end of the experiment and the velocities can be quite accurately determined manually. Next, it was validated on a set of four images acquired at the very early stage of separation, where very slight evidence of separation is detected. Nine images in the middle of the separation were used as a reference. Figure 13 shows last image

from the sequences of nine images in the middle of the separation where it is clear, and the last out of four images at the beginning of separation where separation is not clear. MCR model using three pure components was obtained for the sequence of four images at the beginning of the separation where no separation is visible and for sequence of nine images in the middle of separation. From intersection of the pure component PC3 with PC1 and PC2, ratio of image numbers was calculated which is equal to a ratio of velocities. Ratio of velocities determined by this way from the sequence of nine images with clear separation by MCR was 1.25. The ratio obtained from MCR results of four images with no clear separation is 1.30. Even at very short time of experiment, MCR detected the separation between species and provided the ratio of velocities. This represents

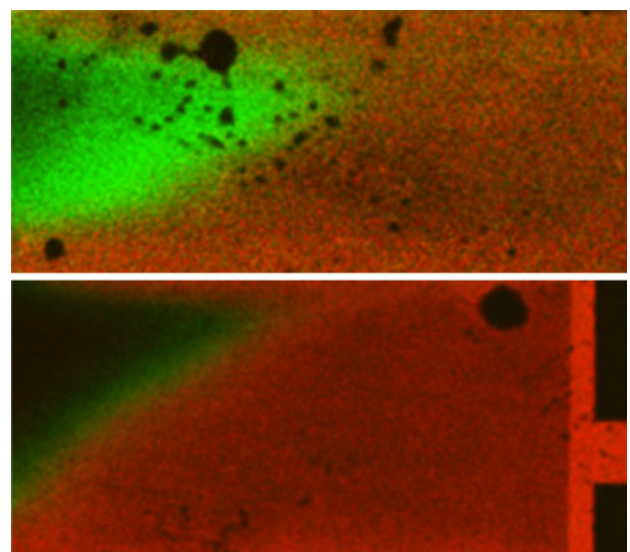


Fig. 13 RGB images. *Top* Last image out of nine acquired in the middle of separation—separation between green and red channels is clear. *Bottom* Last image out of four acquired at the very beginning of separation—separation is barely visible

Table 4 Advances of the proposed methodology over existent manual techniques

Property	Manual calculations	Proposed methodology
(1) Number of images required	As many as necessary for separation to be visible	4
(2) Number of channels to acquire	2, one for each type of florescent region	Any 1
(3) Identification of separation	Yes, if sufficient time is allowed to observe the separation	Yes, in less than a minute
(4) Need to fluorescently label	Yes	No
(5) Accurate absolute velocity	Only, if images of high quality	More accurate than manual
(6) Accurate ratio of velocity	Only, if images of high quality	Yes, regardless from image quality
(7) Speed of calculations	Time-consuming to plot manual profiles and calculate distances from them	Very fast, a few minutes
(8) Problem of uneven profiles	Hard to deal with—need to average multiple profiles	Not a problem, as overall image intensity is an input into algorithm

another very useful capability of optimizing time required to run separation for.

3.4 Advances of the proposed methodology versus existent approaches

Table 4 compares properties of manual calculations of velocities, which are currently being used, to the proposed methodology based on multivariate image analysis. Benefits of the developed approach are quite obvious. A sequence of as few as four images (1), acquired by any single fluorescent channel (2), at the very beginning of the experiment (3), capturing separation of two species with no labeling required (4), provides a data set for successful identification of separation (3) and accurate absolute velocities (5) and very accurate ratio of velocities (6) in a matter of minutes (7) with very limited image preprocessing required (8).

In this study, the velocities of two dyes differed from each by as low as 18%. It is however necessary to study the sensitivity and limits of this methodology toward separation of very similar species. These studies are underway.

4 Conclusions

Multivariate analysis methods such as MCR showed to be successful in providing a time equivalent of moving fronts within array of nanochannels. From MCR results, a criterion was determined that can be used to calculate velocities of two dyes separating within nanochannels. The methodology relies upon an accurate determination of distance traveled by each dye. The ratio of velocities of faster- and slower-moving dyes within nanochannels determined from MCR represents much more accurate ratio than that obtained manually.

The reported results suggest that identification of the transport velocity of different molecular species, even those tagged with the same fluorophore, and thus their

tendency toward separation, can be accomplished the use of multivariate image analysis techniques. Even though fluorescence microscopy is likely to be of limited utility in allowing unambiguous identification of different molecular species, we firmly believe that image analysis methods can yield significant information on transport processes of complex mixtures within nanochannel arrays. This methodology allows for significant extension of studies of flow of mixtures of compounds without the necessity to acquire all emitting wavelengths. Moreover, we suggest that conventional light microscopy can be also used to capture separation of species.

Moreover, the method offers unprecedented advantage in that when different species are simultaneously moving through the medium, the velocity determination can be made before there is any visual separation of the species in the medium.

The capability of the methodology to detect the separation of species and provide a ratio of their velocities at the very early stage of separation will assist in optimizing separation experiments and facilitate fast detection of analytes based on micro- and nano-fluidics assays (US patent US20090148001).

Acknowledgment This study was supported by the Center for Biomedical Engineering (CBME) at UNM, NM DTRA HDTRA1-06-CWMDBR and NSF Sensors CTS-0332315.

References

- Adams MJ (1995) Chemometrics in analytical spectroscopy. Royal Society of Chemistry, Cambridge
- Artyushkova K, Lopez GP, Bore M. Method for multivariate image analysis of confocal temporal image sequences for velocity estimation. US patent US20090148001
- Bellan LM, Craighead HG, Hinestroza JP (2007) Direct measurement of fluid velocity in an electrospinning jet using particle image velocimetry. *J Appl Phys* 102(9):094308-1–094308-5
- Bergsma CBJ et al (2001) Velocity estimation of spots in three-dimensional confocal image sequences of living cells. *Cytometry* 43(4):261–272

- de Juan A et al (2004) Spectroscopic imaging and chemometrics: a powerful combination for global and local sample analysis. *TRAC Trends Anal Chem* 23(1):70–79
- Dittrich PS, Schwille P (2002) Spatial two-photon fluorescence cross-correlation spectroscopy for controlling molecular transport in microfluidic structures. *Anal Chem* 74(17):4472–4479
- Eigenvector Research, I., *PLS_Toolbox* 4.3
- Garcia AL et al (2005) Electrokinetic molecular separation in nanoscale fluidic channels. *Lab Chip* 5(11):1271–1276
- Grega L et al (2007) Flow characterization of a polymer electronic membrane fuel cell manifold and individual cells using particle image velocimetry. *J Fuel Cell Sci Technol* 4(3):272–279
- Gurden SP et al (2003) Analysis of video images from a gas-liquid transfer experiment: a comparison of PCA and PARAFAC for multivariate image analysis. *J Chemometr* 17(7):400–412
- Horn BKP, Schunck BG (1993) Determining optical flow—a retrospective. *Artif Intell* 59(1–2):81–87
- Jaumot J, Vives M, Gargallo R (2004) Application of multivariate resolution methods to the study of biochemical and biophysical processes. *Anal Biochem* 327(1):1–13
- Lowry M, He Y, Geng L (2002) Imaging solute distribution in capillary electrochromatography with laser scanning confocal microscopy. *Anal Chem* 74:1811–1818
- Malinowski ER (1991) *Factor analysis in chemistry*. Wiley, New York
- Markov DA et al (2004) Noninvasive fluid flow measurements in microfluidic channels with backscatter interferometry. *Electrophoresis* 25(21–22):3805–3809
- MATLAB: The Language of Technical Computing. The Mathworks, Inc., Natick, MA
- MCR-ALS, <http://www.ub.edu/mcr/ndownload.htm>
- Natrajan VK, Christensen KT (2007) Microscopic particle image velocimetry measurements of transition to turbulence in micro-scale capillaries. *Exp Fluids* 43(1):1–16
- Oh YJ et al (2009) Effect of wall-molecule interactions on electrokinetic transport of charged molecules in nanofluidic channels during FET flow control. *Lab Chip* 9(11):1601–1608
- Petsev DN (2005) Theory of transport in nanofluidic channels with moderately thin electrical double layers: effect of the wall potential modulation on solutions of symmetric and asymmetric electrolytes. *J Chem Phys* 123(24):244907-1–244907-12
- Sahouria E, Zakhor A (1999) Content analysis of video using principal components. *IEEE Trans Circ Syst Video Technol* 9(8):1290–1298
- Sinton D (2004) Microscale flow visualization. *Microfluid Nanofluid* 1(1):2–21
- Tagliasacchi M (2007) A genetic algorithm for optical flow estimation. *Image Vis Comput* 25(2):141–147
- Tauler R, Smilde A, Kowalski B (1995) Selectivity, local rank, 3-way data-analysis and ambiguity in multivariate curve resolution. *J Chemometr* 9(1):31–58
- Windig W, Guilment J (1991) Interactive self-modeling mixture analysis. *Anal Chem* 63(14):1425–1432
- Yuan Z et al (2007) Electrokinetic transport and separations in fluidic nanochannels. *Electrophoresis* 28(4):595–610